

# Protective Effect and Mechanism of Action of Rosmarinic Acid on Radiation-Induced Parotid Gland Injury in Rats

Dose-Response:  
An International Journal  
January-March 2020:1-11  
© The Author(s) 2020  
Article reuse guidelines:  
sagepub.com/journals-permissions  
DOI: 10.1177/1559325820907782  
journals.sagepub.com/home/dos



Tingting Zhang<sup>1</sup>, Chang Liu<sup>1</sup>, Shanshan Ma<sup>1</sup>, Yirong Gao<sup>1</sup>,  
and Rensheng Wang<sup>1</sup>

## Abstract

The parotid glands are damaged by oxidative stress and a series of pathophysiological changes after irradiation. Rosmarinic acid (RA) is a natural antioxidant that provides a radioprotective effect against harmful damage from ionizing radiation. The present study aims to explore the protective effects of RA on radiation-induced parotid gland injury and its underlying mechanism. Sprague-Dawley rats were irradiated with 15 Gy X-ray and treated with different concentrations of RA (30, 60, and 120 mg/kg) or amifostine (AMI, 250 mg/kg). Saliva secretion function, oxidative stress, apoptosis, the inflammatory response, and fibrosis were determined by the measurement of the salivary flow rate, enzyme-linked immunosorbent assay, transferase-mediated DUTP Nick end labeling, Western blot, quantitative real time polymerase chain reaction, and hematoxylin and eosin staining. Here, we show that RA treatment significantly attenuated reactive oxygen species by a direct hindrance effect and the indirect activation of peroxisome proliferator-activated receptor gamma coactivator 1-alpha/nicotinamide adenine dinucleotide phosphate oxidase 4 signaling. Rosmarinic acid not only reduced apoptosis by inhibiting p53/jun N-terminal kinase activation but also reduced parotid gland tissue fibrosis by downregulating inflammatory factor levels. Compared to AMI, RA has the obvious advantages of late efficacy and convenient usage. Moreover, 60 mg/kg is the minimum effective dose of RA. Therefore, RA can potentially be applied as a therapeutic radioprotective agent to treat radiation-induced parotid gland injury in the future.

## Keywords

rosmarinic acid, parotid gland, radiation injury, oxidative stress, apoptosis, fibrosis

## Introduction

Head and neck cancer (HNC) is the seventh most common group of cancers in the world.<sup>1</sup> The global incidence of HNC is more than 5 million cases per year, and the annual incidence in China is approximately 135 000 cases.<sup>2</sup> Radiotherapy is one of the major treatments for patients with HNC and has achieved good therapeutic effects.<sup>3</sup> However, patients with HNC inevitably have several complications because of radiation damage to normal tissues.<sup>4</sup> Xerostomia, which is due to radiation-induced salivary gland injury, is the most common persistent oral sequela.<sup>5</sup> It persists for several years or even the rest of the patient's life, and seriously affects the patient's quality of life.<sup>6</sup>

Oxidative stress is a special state of cellular stress after exposure to irradiation (IR) and results in the production of substances such as oxygen free radicals.<sup>7</sup> Reactive oxygen species (ROS) play an important role in promoting intracellular signal transduction.<sup>8</sup> On the one hand, ROS can activate cellular signaling molecules, regulating different cellular functions,

including energy metabolism, stress response, and growth signals in redox reactions.<sup>9</sup> Moreover, ROS regulate cell death and growth.<sup>10</sup> Excessive ROS attenuate the antioxidant capacity of cells through oxidative stress, which further leads to severe cellular damage.<sup>11</sup> Reactive oxygen species are regarded as crucial players in radiation-induced salivary gland tissue injury. In vivo and in vitro experiments showed that ROS levels sharply

<sup>1</sup> Department of Radiation Oncology, The First Affiliated Hospital of Guangxi Medical University, Nanning, China

Received 28 October 2019; received revised 2 January 2020; accepted 19 January 2020

## Corresponding Author:

Rensheng Wang, Department of Radiation Oncology, The First Affiliated Hospital of Guangxi Medical University, No. 6 Shuangyong Road, Nanning 530021, China.

Email: 13807806008@163.com



increase in salivary glands after IR.<sup>12</sup> At present, many radioprotectants prevent IR damage by inhibiting oxidative stress.

Several years ago, amifostine (AMI) was shown to reduce xerostomia in patients with HNC undergoing radiotherapy and was the first cytoprotective agent approved by the United States Food and Drug Administration.<sup>13</sup> However, AMI has limited clinical use due to its high cost and adverse reactions, namely, nausea and vomiting, low blood pressure, lethargy, chills, and allergic symptoms.<sup>14</sup> Many patients who simultaneously undergo chemotherapy and radiotherapy have a difficult time enduring these adverse reactions. Therefore, there is still a lack of low toxicity and highly effective radioprotectants that can prevent salivary gland injury following IR. In recent years, plant-derived antioxidants have attracted increasing attention not only because they effectively protect against radiation-induced salivary gland injury but also because they have low toxicity and a lower cost.<sup>15,16</sup> In our previous study, we found that a water extract of *Sarcandra glabra* had protective effects against radiation-induced parotid gland damage in Guinea pigs. The continued administration of *S glabra* following IR reduced the content of malondialdehyde in parotid gland tissues and simultaneously protected parotid gland tissues against  $\gamma$ -ray-induced oxidative stress and acute radiation damage.

Rosmarinic acid (RA), which is a water-soluble natural phenolic compound, is one of the main active ingredients of *S glabra* and is widely present in various plants.<sup>17</sup> Rosmarinic acid has multiple pharmacological activities, including anti-inflammatory,<sup>18</sup> antiangiogenic,<sup>19</sup> and anticancer.<sup>20</sup> In particular, it is a natural antioxidant<sup>21</sup> that can compete with unsaturated fatty acids for binding to lipid peroxyl groups to terminate the chain reaction of lipid peroxidation and reduce the rate of lipid peroxidation. The ability of RA to scavenge radiation-induced ROS and prevent free radical-induced cell damage is stronger than that of many other natural antioxidants, such as caffeic acid, chlorogenic acid, and folic acid.<sup>22,23</sup> Rosmarinic acid provides a radioprotective effect against the harmful damage induced by ionizing radiation.<sup>24</sup> In the present study, we used a rat model of local exposure to IR to assess whether RA can attenuate radiation-induced parotid gland injury and clarify the possibly influenced biomarkers and mechanisms in vivo.

## Materials and Methods

### Animals

This study was approved by the Committee on the Ethics of Animal Experiments of Guangxi Medical University (permit no. 201711014; Nanning, China). A total of 240 male specific pathogen-free Sprague-Dawley rats (9 weeks old, weighing  $230 \pm 20$  g) were purchased from the Laboratory Animal Center of Guangxi Medical University. The rats were housed in suspended plastic cages at 22°C to 24°C and 50% to 60% humidity on a 12-hour light/dark cycle. Food and water were provided ad libitum. The rats were randomly divided into 6 groups: the control (Ctrl) group, the (IR alone) group, the IR + 30, 60, and 120 mg/kg RA (IR and 30, 60, and 120 mg/kg RA, respectively) groups, and the

IR + AMI (irradiation and amifostine) group. Rosmarinic acid (Shanghai Yuanye Biotechnology, Shanghai, China) was compounded with saline and was intragastrically administered 7 days before IR and until the rats were sacrificed. Amifostine (Sigma-Aldrich, St. Louis, MO; 250 mg/kg body weight in 1 mL saline solution) was intraperitoneally administered 30 minutes before IR, which is effective and well tolerated by rats to prevent saliva-flow dysfunction according to the previous research.<sup>25</sup> Eight rats from each group were randomly sacrificed at each time point (the 3rd, 10th, 30th, 60th, and 120th day after IR).

### Radiation Exposure

All rats were fixed to a plane board after being anesthetized. The rats in the IR group, the IR + 30, 60, and 120 mg/kg RA groups, and the IR + AMI group received a single dose of 15 Gy by a 6 MeV electron beam radiation delivered by a linear accelerator (Varian Clinac iX, Varian Medical Systems Inc, Palo Alto, CA). The rats were irradiated from the upper edge of the retroauricular region to the sternum manubrium, including all potential parotid gland tissues in the neck field (Source-skin distance = 100 cm, field size = 5 cm  $\times$  3 cm, dose rate = 400 MU/min, 5-mm bolus above the neck). The other parts of the body were shielded by a lead block.

### Salivary Flow Rate Measurement

Rats were injected intraperitoneally with 0.6 mg/kg pilocarpine hydrochloride (Sigma-Aldrich), and then stimulated saliva was collected 4 days before and 3, 10, 30, 60, and 120 days after IR according to a previously described procedure.<sup>26</sup> Cotton balls, which were preweighed and kept in the oral cavity for 10 minutes to absorb saliva, were immediately weighed on an electronic balance to prevent moisture loss. Assuming the specific gravity of saliva to be 1.0 g/cm<sup>3</sup>, the difference of pre and postcollection cotton ball mass in grams was substituted by milliliters. The salivary flow rate (SFR) was calculated as the ratio of the saliva volume to the collection time ( $\mu$ L/min).

### Quantitative Real Time Polymerase Chain Reaction

Total RNA was extracted from the parotid gland tissues using a TRIzol plus kit (Invitrogen, Carlsbad, CA) for complementary DNA (cDNA) synthesis. Synthesized cDNA was used for quantitative real time polymerase chain reaction (qRT-PCR) analysis using an Applied Biosystems 7500 Real Time Polymerase Chain Reaction System (Life Technologies, Waltham, MA) following the manufacturer's instructions to detect the messenger ribonucleic acid (mRNA) expression levels of peroxisome proliferator-activated receptor gamma coactivator 1-alpha (PGC1- $\alpha$ ) and nicotinamide adenine dinucleotide phosphate oxidase 4 (NOX4), mouse double minute 2 (MDM2), BCL2-associated X (Bax), B-cell lymphoma 2 (Bcl-2), p53, Caspase-3, Col1a1, Col1a2, and Col3a1. All the mRNA levels were determined by the  $2^{-\Delta\Delta C_t}$  method, and  $\beta$ -actin was used as an internal control for normalization. The primer sequences used for qRT-PCR are shown in Table 1.

**Table 1.** Primer Sequences.

Gene	Primer Sequences	Annealing Temperature (°C)	Product Length (bp)	Accession Numbers
PGC-1 $\alpha$ -F	ACAACCGCAGTCGCAACATG	62.12	174	NM_031347.1
PGC-1 $\alpha$ -R	TGAGGAGGAGTCGTGGGAGG	62.50		
NOX4-F	ATTGTCCCAGTGTATCAGCA	56.53	139	NM_053524.1
NOX4-R	GGAGGCAGTAGTAAATCTCG	55.09		
MDM2-F	CTTGATGATGGCGTAAGTGA	55.57	176	NM_001108099.1
MDM2-R	TGATAGACTGTGACCCGATA	54.78		
p53-F	GTATGCTGAGTATCTGGACGACA	59.68	170	NM_030989.3
p53-R	CCAGCGTGATGATGGTAAGG	58.41		
Bax-F	TGCTACAGGGTTTCATCCAGG	59.72	113	NM_017059.2
Bax-R	GAGACACTCGCTCAGCTTCTTG	61.24		
Bcl-2-F	TGTGGCCTTCTTTGAGTTCC	58.41	149	LI4680.1
Bcl-2-R	CATCCAGCCTCCGTTATCC	59.96		
Caspase-3-F	GAAAGCATCCAGCAATAGGC	57.21	125	NM_012922.2
Caspase-3-R	AGCGATGACTCAGCACCTCC	61.95		
Colla1-F	TACAGCACGCTTGTGGATGG	60.67	194	NM_053304.1
Colla1-R	CAGATTGGGATGGAGGGAGTT	59.15		
Colla2-F	AGGAGGCTATGACTTTGGTTTCG	60.62	170	NM_053356.1
Colla2-R	TGCGGGCAGGGTCTTTCTA	61.49		
Col3a1-F	GCCTCCCAGAACATTACATACC	58.52	192	NM_032085.1
Col3a1-R	TGTCTTGCTCCATTACCAG	57.81		
$\beta$ -actin-F	CGTAAAGACCTCTATGCCAACA	58.14	100 bp	NM_031144.3
$\beta$ -actin-R	TAGGAGCCAGGGCAGTAATC	58.58		

Abbreviations, Bax, BCL2-associated X; Bcl-2, B-cell lymphoma 2; MDM2, mouse double minute 2; NOX4, nicotinamide adenine dinucleotide phosphate oxidase 4; PGC1- $\alpha$ , peroxisome proliferator-activated receptor gamma coactivator 1-alpha.

### Western Blot Analysis

Parotid gland tissues (30 mg) were homogenized in 200 to 400  $\mu$ L Radioimmunoprecipitation assay-phenylmethanesulfonyl fluoride lysis buffer (Solarbio, Beijing, China). The concentration of the supernatant was detected using a bicinchoninic acid assay kit (Solarbio). The samples were boiled at 100°C for 10 minutes before electrophoresis. After electrophoresis, the proteins were transferred to polyvinylidene fluoride membranes (Millipore, Bedford, MA). Then, the membranes were blocked using 8% nonfat milk in TBST buffer (50 mm Tris-HCl, 100 mm NaCl, and 0.1% Tween-20, pH 7.4) for 3 hours. Then, the membranes were immunoblotted with one of the following antibodies: phosphorylated c-jun N-terminal kinase (p-JNK; Abcam, Cambridge, United Kingdom), jun N-terminal kinase (JNK; Abcam), phosphorylated c-Jun (p-c-Jun; Abcam), c-Jun (c-Jun; Abcam), PGC1- $\alpha$  (Abcam), NOX4 (Abcam), MDM2 (Abcam), Bax (Abcam), Bcl-2 (Abcam), p53 (Abcam), Caspase-3 (Abcam), Collagen I, Collagen III, and  $\beta$ -actin (Abcam). All blots were developed using the ECL Western Blotting Detection Kit Reagent (Solarbio) and detected using a gel imaging analysis system (Tanon 5200, Image Quant LAS 4000 mini, GE, Piscataway, NJ).

### Measurement of ROS and Total Antioxidant Capacity Levels, Enzyme-Linked Immunosorbent Assay

Parotid gland tissues were rapidly removed, thoroughly homogenized and centrifuged at 5000 rpm/min for 10 minutes. The supernatant was assayed in accordance with the manufacturer's

instructions for the Rat Reactive Oxygen Species Cluster Kit (Mlbio, Shanghai, China). The optical density value for each specimen was determined by a microplate reader at 450 nm (FilterMax F3, Molecular Devices Corporation, San Francisco, CA). Samples for total antioxidant capacity (T-AOC) detection were homogenized and centrifuged at 10 000 rpm/min for 5 minutes. The supernatant was assayed in accordance with the manufacturer's instructions for the T-AOC Kit (Solarbio). The optical density value for each specimen was determined by a microplate reader at 593 nm (MD, FilterMax F3). According to the manufacturer's instructions, the levels of tumor necrosis factor-alpha (TNF- $\alpha$ ), interleukin (IL)-6, and IL-2 in the rat serum were determined using a TNF- $\alpha$  enzyme-linked immunosorbent assay (ELISA) kit (R&D, Sao paulo, MN), an IL-6 ELISA kit (R&D), and an IL-2 ELISA kit (R&D), respectively.

### Hematoxylin and Eosin Staining Analysis

Thin slices of tissues from all samples were delivered to our histopathology department and were fixed in 4% formaldehyde solution (pH 7.0). After rehydration and deparaffinization, 5- $\mu$ m longitudinal sections were stained with hematoxylin solution for 5 minutes, dipped 5 times in 1% acid ethanol (1% HCl in 70% ethanol) and then washed with double-distilled water. Then, the sections were stained with eosin solution for 3 minutes. Finally, dehydration, permeabilization, and sealing were performed. The results were independently evaluated in a blinded manner by 2 pathologists.

**Table 2.** Salivary Flow Rate ( $\mu\text{L}/\text{min}$ ).<sup>a</sup>

	-4 Days	3 Days	10 Days	30 Days	60 Days	120 Days
Ctrl	130.5 $\pm$ 7.62	139.01 $\pm$ 9.44	142.38 $\pm$ 7.73	161.63 $\pm$ 9.09	174.63 $\pm$ 7.31	188.5 $\pm$ 8.83
IR	129.00 $\pm$ 12.24	100.88 $\pm$ 8.79 <sup>b</sup>	91 $\pm$ 5.76 <sup>b</sup>	93.88 $\pm$ 8.76 <sup>b</sup>	89.13 $\pm$ 5.3 <sup>b</sup>	84.13 $\pm$ 5.51 <sup>b</sup>
IR+30 mg/kg RA	129.01 $\pm$ 8.33	104.13 $\pm$ 7.34 <sup>b</sup>	104.63 $\pm$ 5.5 <sup>b,c</sup>	126 $\pm$ 8.5 <sup>b,c</sup>	127.13 $\pm$ 6.81 <sup>b,c</sup>	132.13 $\pm$ 10.01 <sup>b,c</sup>
IR+60 mg/kg RA	127.63 $\pm$ 8.01	118.63 $\pm$ 6.76 <sup>b,c,d</sup>	116.88 $\pm$ 6.22 <sup>b,c,d</sup>	142.13 $\pm$ 7.64 <sup>b,c,d</sup>	141.38 $\pm$ 9.64 <sup>b,c,d</sup>	152.88 $\pm$ 11.41 <sup>b,c,d</sup>
IR+120 mg/kg RA	131.13 $\pm$ 9.23	124.13 $\pm$ 5.44 <sup>b,c,d</sup>	117.75 $\pm$ 5.44 <sup>b,c,d</sup>	144 $\pm$ 7.71 <sup>b,c,d</sup>	143.13 $\pm$ 9.67 <sup>b,c,d</sup>	152.25 $\pm$ 10.36 <sup>b,c,d</sup>
IR+AMI	130.63 $\pm$ 10.13	112.5 $\pm$ 4.75 <sup>b</sup>	115.38 $\pm$ 4.98 <sup>b,c,d</sup>	143.01 $\pm$ 9.8 <sup>b,c,d</sup>	146.25 $\pm$ 9.84 <sup>b,c,d</sup>	160.5 $\pm$ 8.12 <sup>b,c,d</sup>

Abbreviations: AMI, amifostine; Ctrl, control; IR, irradiation; RA, rosmarinic acid.

<sup>a</sup>The data are represented as the means  $\pm$  SDs ( $n = 8$ ).

<sup>b</sup>Values significantly ( $P < .05$ ) differ from the Ctrl group.

<sup>c</sup>Values significantly ( $P < .05$ ) differ from the IR group.

<sup>d</sup>Values significantly ( $P < .05$ ) differ from the IR+30 mg/kg RA group.

### Terminal Deoxynucleotidyl Transferase-Mediated DUTP Nick End Labeling Staining Analysis

A transferase-mediated DUTP Nick end labeling (TUNEL) Assay kit (Abcam) was used to detect apoptotic cells. According to the kit manufacturer's instructions, fixed samples were treated with hydrogen peroxide for 10 minutes at room temperature to inactivate endogenous peroxidases and permeabilized with 0.1% Triton X-100 in 0.1% sodium citrate for 5 minutes on ice. The samples were exposed to terminal deoxynucleotidyl transferase solution for 1 hour at 37°C. After the addition of chromogenic 3,3'-diaminobenzidine, the samples were washed, dehydrated, permeabilized, and sealed. The number of TUNEL-positive stained cells was counted using optical microscopy (Olympus, Tokyo, Japan).

### Statistical Analysis

The data are expressed as the means  $\pm$  standard deviations and analyzed by one-way analysis of variance, followed by multiple comparison test using SPSS version 25.0 (SPSS Inc, Chicago, IL). Statistical significance was set at  $P < .05$ .

## Results

### Rosmarinic Acid Prevents Radiation-Induced Hyposalivation

To investigate the effects of RA on saliva secretion function, the SFR was determined. Within 120 days, the SFR in the IR group decreased compared to that in the Ctrl group (Table 2,  $P < .05$ ). The administration of 60 mg/kg and 120 mg/kg RA effectively prevented the reduction in the SFR in irradiated rats from 3 days to 120 days post-IR (Table 2,  $P < .05$ ), whereas AMI has no significant effect on saliva secretion function at the very early stage (Table 2, IR vs IR + AMI, 3 days,  $P > .05$ ). At day 10, 30, 60, and 120 after IR, the difference in the SFR was not statistically significant among the IR + 60 mg/kg RA group, IR + 120 mg/kg RA group, and IR + AMI group ( $P > .05$ ). Higher levels of SFRs in the IR + 60 mg/kg RA group and IR + 120 mg/kg RA group in compared to IR + 30 mg/kg RA group at different time points (Table 2,  $P < .05$ ; Figure 1).

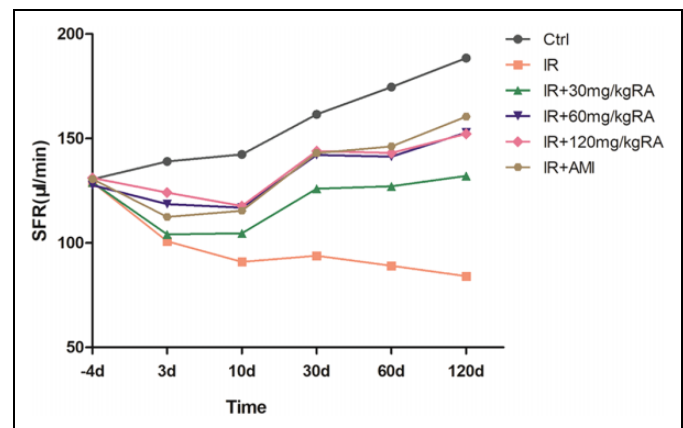


**Figure 1.** Effect of rosmarinic acid on the salivary flow rate. Stimulated saliva was collected from each group 4 days before and 3, 10, 30, 60, and 120 days after irradiation ( $\mu\text{L}/\text{min}$ ,  $n = 8$  per group). AMI indicates amifostine; Ctrl, control; IR, irradiation; RA, rosmarinic acid; SFR, salivary flow rate.

### Rosmarinic Acid Inhibited the Oxidative Stress Reaction in the Irradiated Parotid Gland

To explore the relationship between oxidative stress reaction and the suppression of radiation-induced parotid gland hyposalivation by RA, the ROS and T-AOC levels were examined (Figure 2A); PGC1- $\alpha$  and NOX4 were also examined by Western blot and RT-PCR (Figure 2B and C). We observed that compared to those in the Ctrl group, the T-AOC levels and the protein and mRNA expression of PGC1- $\alpha$  were decreased substantially in the IR group, whereas ROS levels and the expression of NOX4 were increased at the same time point (Figure 2A-C). Reactive oxygen species level peaked at day 10 after IR (Figure 2A). Furthermore, the application of RA alleviated the post-IR changes in ROS and T-AOC levels, the protein and mRNA expression of PGC1- $\alpha$  and NOX4 in the IR + 60 mg/kg RA group and IR + 120 mg/kg RA group, as in the IR + AMI group. There was no statistically significant difference among these three groups. Moreover, drug suppression of oxidative stress reaction factors in these 3 groups was more effective than that in the IR + 30 mg/kg RA group (Figure 2A-C).

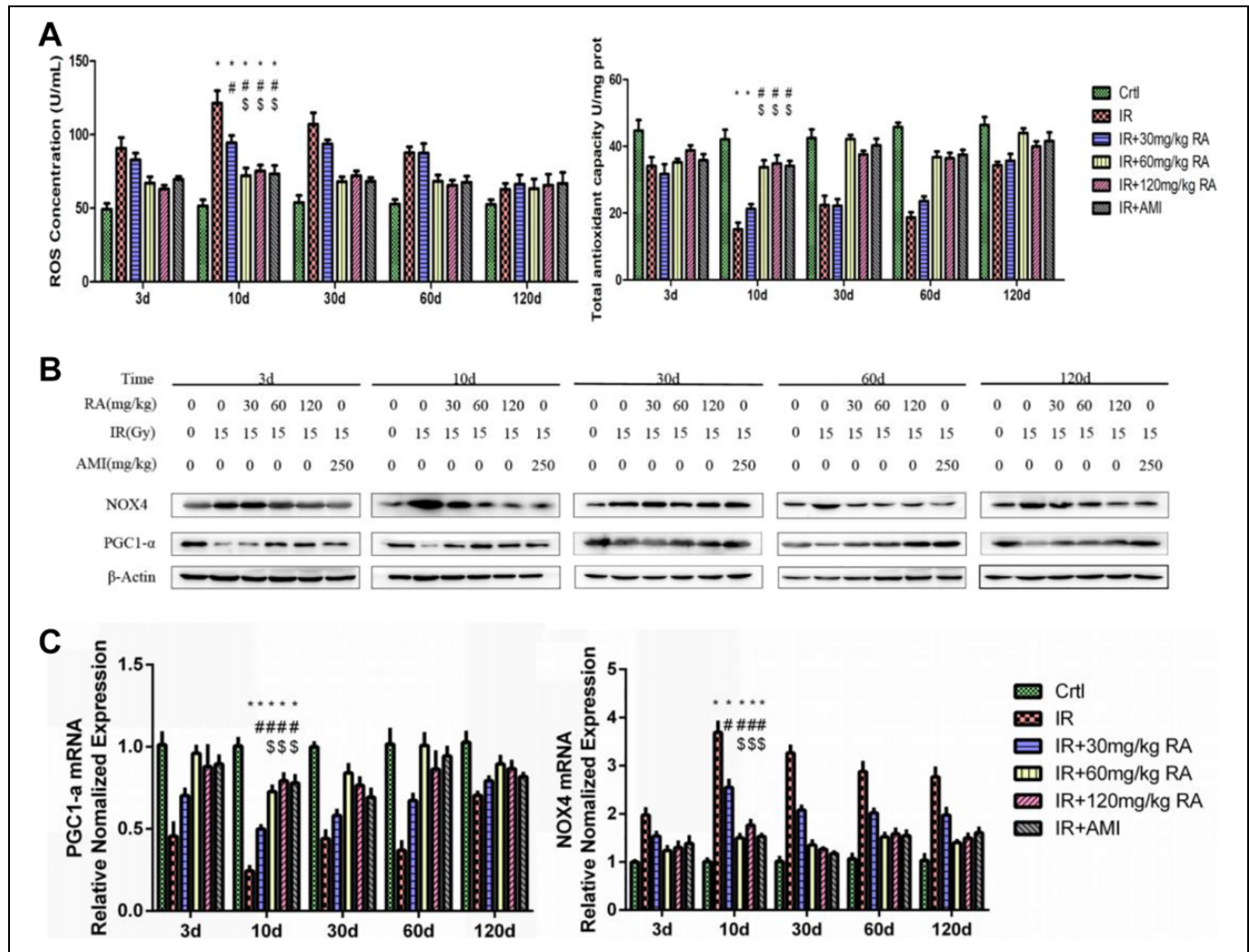


**Figure 2.** Effect of rosmarinic acid on the oxidative stress reaction. Reactive oxygen species and total antioxidant capacity levels were determined (A). PGC1- $\alpha$  and NOX4 were examined by Western blotting (B) and real-time polymerase chain reaction (C). \* Values significantly ( $P < .05$ ) differ from the Ctrl group. # Values significantly ( $P < .05$ ) differ from the IR group. \$ Values significantly ( $P < .05$ ) differ from the IR+30 mg/kg RA group. AMI indicates amifostine; Ctrl, control; IR, irradiation; NOX4, nicotinamide adenine dinucleotide phosphatase4; PGC1- $\alpha$ , peroxisome proliferator-activated receptor gamma coactivator 1-alpha; RA, rosmarinic acid.

### Rosmarinic Acid Suppressed Radiation-Induced Parotid Gland Apoptosis

In our study, parotid gland apoptosis was investigated by TUNEL staining. The positive cells were mostly acinar cells (Figure 3B, red arrow). The results showed that the apoptosis rates of parotid gland cells reached the highest level 30 days post-IR in the IR group (Figure 3A). More inhibition of apoptosis rates were in the IR + 60 mg/kg RA group, IR + 120 mg/kg RA group, and IR + AMI group than in the IR + 30 mg/kg RA group from 10 days to 60 days post-IR (Table 3,  $P < .05$ ). There were no significant differences among the former 3 groups (Table 3,  $P > .05$ ).

Because of endogenous enzymatic activity, TUNEL staining may be not reliable in the parotid glands. Figure 3D showed that compared to that in the Ctrl group, the mRNA expression of p53 was significantly increased in the IR group and peaked

at day 10 after IR; Bax and Caspase-3 were also increased and peaked at day 30 after IR; meanwhile, Bcl-2 and MDM-2 were significantly decreased. Importantly, we observed that treatment with RA sharply reduced the expression of p-JNK, p-c-Jun, p53, Bax and Caspase-3, whereas increased the expression of Bcl-2 and MDM-2. These results indicated that RA blocked the apoptotic signaling pathway in parotid glands upon IR (Figure 3C and D).

### Rosmarinic Acid Inhibited Interstitial Hyperplasia in the Radiation-Exposed Parotid Gland in the Late Stage Through Its Anti-Inflammatory Effect

Hematoxylin and eosin (HE) staining results showed that in the Ctrl group, there were intensive congenic serous secretory acini (Figure 4A). Conversely, the parotid glands in the IR

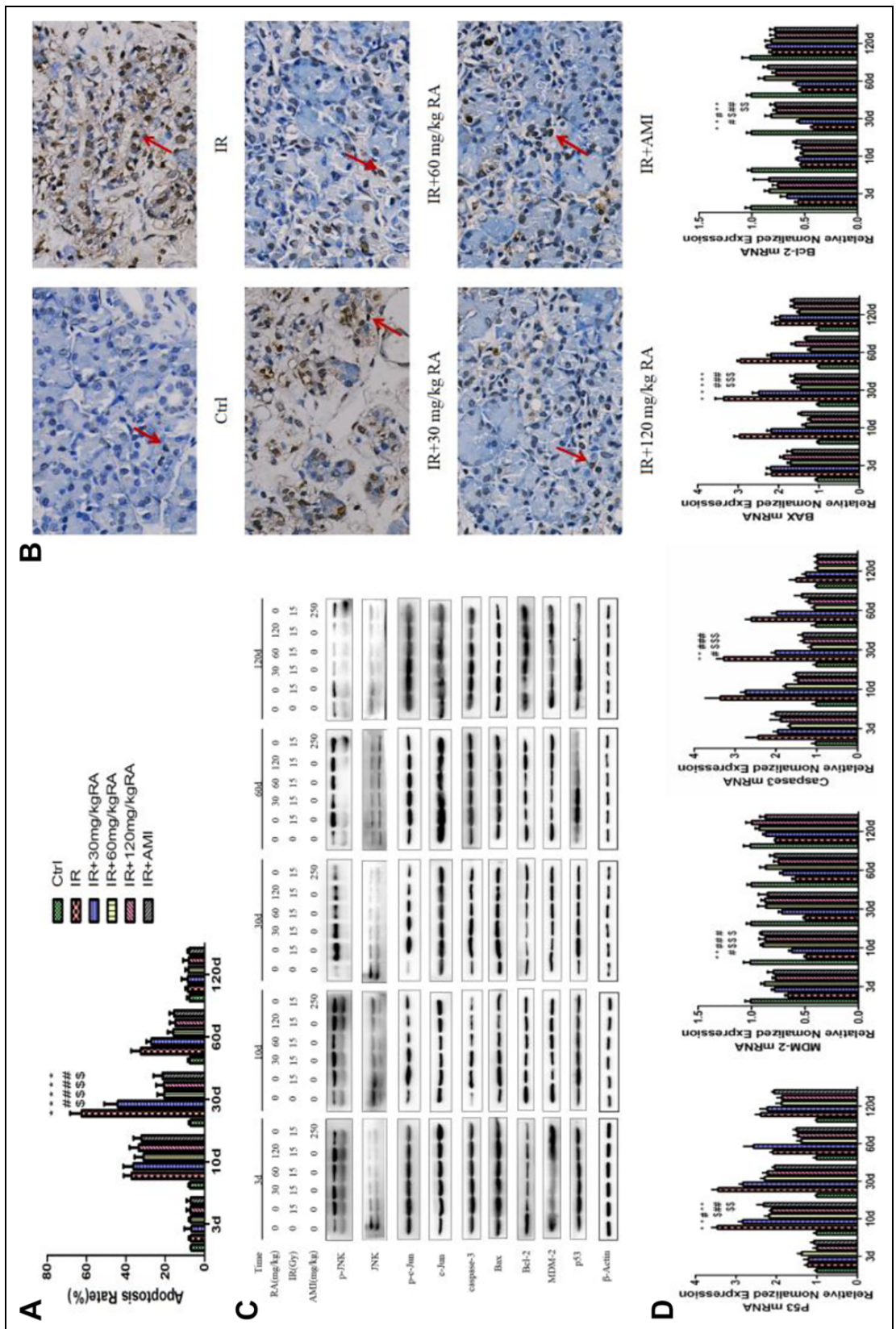


**Figure 3.** Effect of rosmarinic acid on apoptosis. The apoptosis rate was calculated as the ratio of the number of TUNEL positive cells relative to the number of total cells (%). \* Values significantly ( $P < .05$ ) differ from the Ctrl group. # Values significantly ( $P < .05$ ) differ from the IR group. \$ Values significantly ( $P < .05$ ) differ from the IR+30 mg/kg RA group (A). Microscopic images ( $\times 400$ ) showed apoptosis at days 30 postirradiation when the most significant difference among groups occurred. The arrows indicate apoptotic cells (B). The protein of p-JNK, JNK, p-c-Jun, MDM2, Bax, Bcl-2, p53, Caspase-3 were determined by Western blotting (C) and the mRNA expression of p53, MDM2, Caspase-3, Bax, Bcl-2 were determined by real-time polymerase chain reaction (D). AMI indicates amifostine; Bax, BCL2-associated X; Bcl-2, B-cell lymphoma 2; Ctrl, control; IR, irradiation; JNK, jun N-terminal kinase; MDM2, mouse double minute 2; mRNA, messenger ribonucleic acid; p-JNK, phosphorylated c-jun N-terminal kinase; p-c-Jun, phosphorylated c-Jun; RA, rosmarinic acid; TUNEL, transferase-mediated DUTP Nick end labeling.

**Table 3.** Apoptosis Rate (%).<sup>a</sup>

	3 Days	10 Days	30 Days	60 Days	120 Days
Ctrl	6.67 ± 0.49	7.35 ± 0.88	7.09 ± 1.04	7.49 ± 1.11	7.70 ± 1.33
IR	6.95 ± 1.18	37.17 ± 3.97 <sup>b</sup>	62.48 ± 5.86 <sup>b</sup>	32.42 ± 4.93 <sup>b</sup>	8.52 ± 1.28
IR+30 mg/kg RA	6.58 ± 0.71	36.14 ± 5.16 <sup>b</sup>	44.17 ± 6.89 <sup>b,c</sup>	27.07 ± 2.54 <sup>b</sup>	8.51 ± 1.25
IR+60 mg/kg RA	7.2 ± 1.00	31.08 ± 4.58 <sup>b</sup>	20.47 ± 3.53 <sup>b,c,d</sup>	15.82 ± 2.96 <sup>b,c,d</sup>	8.22 ± 1.65
IR+120 mg/kg RA	7.21 ± 0.97	33.58 ± 4.56 <sup>b</sup>	20.66 ± 4.01 <sup>b,c,d</sup>	14.86 ± 2.86 <sup>b,c,d</sup>	8.04 ± 0.90
IR+AMI	7.01 ± 1.14	32.12 ± 4.07 <sup>b</sup>	21.34 ± 4.7 <sup>b,c,d</sup>	15.47 ± 2.36 <sup>b,c,d</sup>	7.75 ± 1.10

Abbreviations: AMI, amifostine; Ctrl, control; IR, irradiation; RA, rosmarinic acid.

<sup>a</sup>The data are represented as the means ± SDs (n = 8).

<sup>b</sup>Values significantly ( $P < .05$ ) differ from the Ctrl group.

<sup>c</sup>Values significantly ( $P < .05$ ) differ from the IR group.

<sup>d</sup>Values significantly ( $P < .05$ ) differ from the IR+30 mg/kg RA group.

group exhibited a significant reduction in acinar number, acinar atrophy, duct luminal dilation, vacuolization, interstitial fibrosis, and capillary congestion. The structure of the glandular lobule disappeared and was replaced by fibrosis tissue, at day 60 after IR, and this was further aggravated at day 120 (Figure 4A). In addition, RA substantially reduced the fibrosis of the parotid glands, but AMI did not have the same effect on fibrosis (Figure 4A). Collagen I and Collagen III are important related indicators of interstitial hyperplasia. The trends of the protein expression of Collagen I and Collagen III (Figure 4B) were as the same as those shown by HE staining. The mRNA expression of Col1a1, Col1a2, and Col3a1 was higher in the IR group than that in the Ctrl group from 30 days to 120 days post-IR (Figure 4C,  $P < .05$ ). Moreover, treatment with 60 mg/kg or 120 mg/kg RA significantly reversed the mRNA overexpression of Col1a1, Col1a2, and Col3a1 after IR in parotid gland tissues at these time points. Amifostine did not have any significant effect on irradiated parotid gland tissues.

Tumor necrosis factor-alpha, IL-2,<sup>27</sup> and IL-6<sup>28</sup> are inflammatory factors that play an important role in the development of interstitial fibrosis. As shown in Figure 4D, the levels of TNF- $\alpha$ , IL-2, and IL-6 were increased after IR in the IR group and peaked 30 days after IR. On the other hand, RA (60 mg/kg and 120 mg/kg) significantly reversed the radiation-mediated changes in these 3 inflammatory factors (Figure 4D,  $P < .05$ ), but 30 mg/kg RA and AMI did not induce such significant changes in parotid gland tissues post-IR.

## Discussion

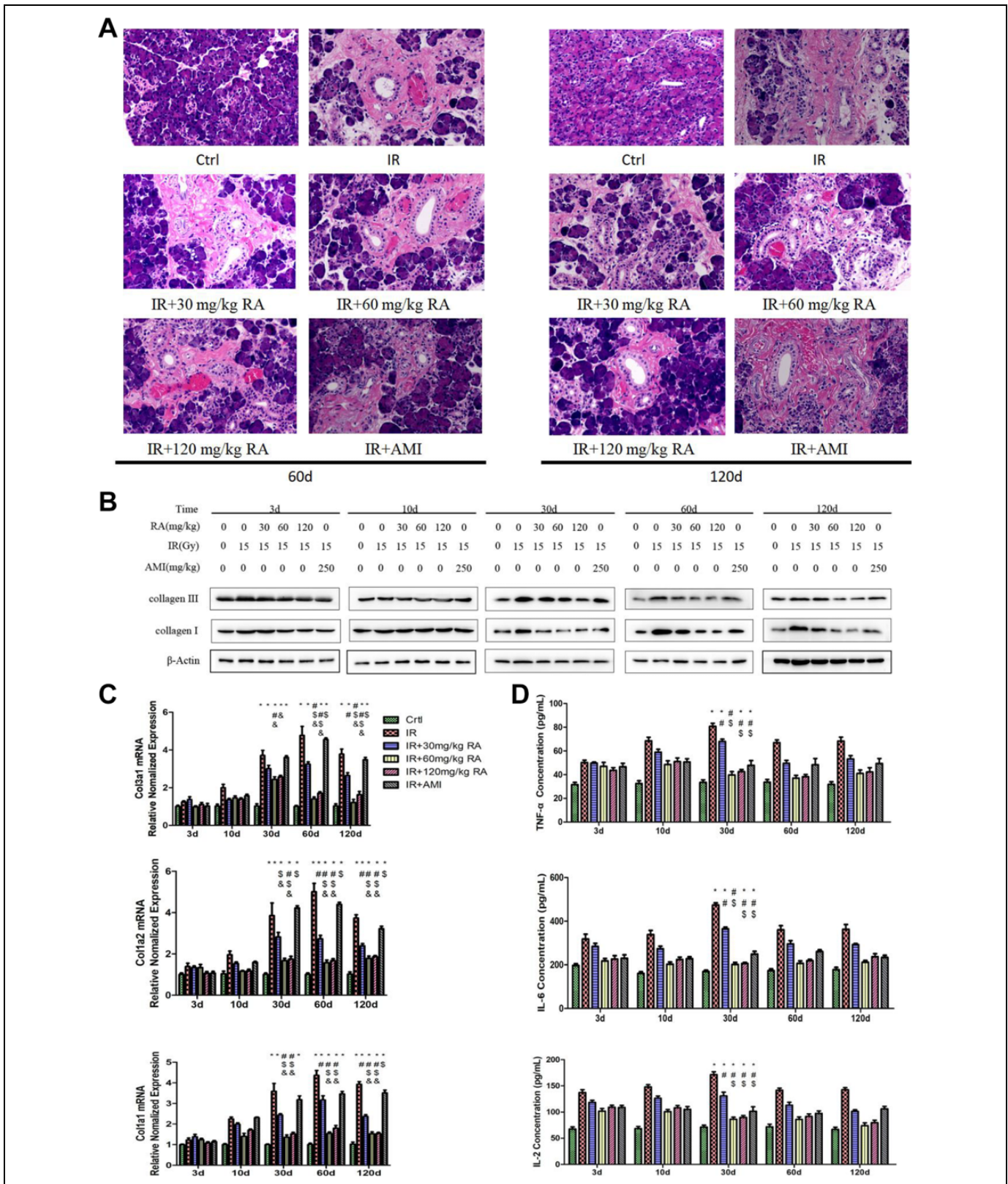
Radiation causes structural damage to acini, ducts, nerves, blood vessels, and lymphatic vessels in the salivary glands, which gradually induces salivary gland hypofunction or a permanent loss of function and ultimately results in xerostomia. There are 3 large salivary glands (the parotid gland, submandibular gland, and sublingual gland) and many small salivary glands in humans. The parotid gland and submandibular gland contribute the majority of saliva volume. As the largest salivary gland, the parotid gland is more sensitive than the submandibular gland to IR.<sup>29</sup> Therefore, parotid gland injury is considered to be the main cause of xerostomia.<sup>30</sup> In the present study, we

focused on radiation-induced parotid gland damage, specifically the inherent association between damage and apoptosis, oxidative stress, inflammation, fibrosis and assessed the possible therapeutic potential of RA against both early and late radiation effects.

During the early stage of radiation-induced damage, ionizing radiation interacts with body components and produces a large amount of ROS by converting water. Reactive oxygen species can destroy cell structures by acting directly or indirectly on DNA, proteins, and lipids and consequently result in apoptosis and necrosis.<sup>31</sup> Our current data showed significant upregulation in ROS production and downregulation in T-AOC levels in IR-exposed parotid gland tissues (Figure 3A), which is in accordance with earlier observations.<sup>32</sup> On the other hand, RA treatment significantly restricted radiation-induced increases in ROS levels (Figure 3A), thereby reducing further oxidative damage. The reasons may be that RA can absorb and neutralize ROS through their catechol structures and that RA has a direct hindrance effect of ROS production.<sup>24,33</sup>

Peroxisome proliferator-activated receptor gamma coactivator 1-alpha is a transcriptional coactivator involved in the control of the oxidative stress pathway and lipid metabolism.<sup>34</sup> Peroxisome proliferator-activated receptor gamma coactivator 1-alpha regulates intracellular redox status by reducing ROS generation and upregulating antioxidant enzymes<sup>35</sup> and regulates the expression of NOX4.<sup>36</sup> Nicotinamide adenine dinucleotide phosphate oxidase 4 is a member of the NOX family, which is a group of oxidatively active proteins in the cell that are widely expressed in various cells and tissues. Nicotinamide adenine dinucleotide phosphate oxidase 4 significantly catalyzes ROS production and affects apoptosis.<sup>37</sup> In this study, IR significantly regulated PGC1- $\alpha$ /NOX4 signaling, as evidenced by the significantly low expression of PGC1- $\alpha$  and the overexpression of NOX4. On the other hand, RA significantly reversed this signaling, and this effect may be associated with the antioxidant and radical-scavenging effect of RA. Moreover, RA indirectly reduced the production of ROS and attenuated oxidative stress.

Earlier investigations revealed that ROS activate apoptosis by modulating the expression of different apoptosis-associated proteins.<sup>38</sup> The overproduction of ROS activates p53 and JNK/



c-JUN and inhibits MDM2.<sup>39</sup> p53, as a genome guardian, can initiate apoptosis when the DNA of cells is damaged and cannot be repaired. Most apoptotic factors depend on the regulation of p53. Mouse double minute 2 is the major negative regulator of p53, regulating it by inhibiting its transcription and promoting its degradation.<sup>40</sup> There is complex regulation between p53 and MDM2 under oxidative stress. The imbalance of these 2 factors leads to apoptosis or growth retardation.<sup>41</sup> Jun N-terminal kinase, as a mitogen-activated protein kinase, plays a central role in ROS-mediated apoptotic signaling. Reactive oxygen species mediate apoptosis by regulating the JNK pathway.<sup>42</sup> Multiple studies have indicated that JNK/c-JUN signaling may initiate apoptosis through the transcription of pro-apoptotic proteins.<sup>43</sup> Jun N-terminal kinase may physically bind to and phosphorylate the pro-apoptotic gene Bcl-2 to trigger Bax-dependent apoptosis.<sup>44,45</sup> B-cell lymphoma 2 is a proto-oncogene that can inhibit apoptosis. Bax, as a Bcl-2 antagonist, belongs to the Bcl-2 gene family. B-cell lymphoma 2 family members can also change the permeability of the mitochondrial membrane and activate the caspase-related apoptotic response. Caspase-3 is the key protease in mammalian apoptosis and is critical for the activation of the caspase cascade.<sup>46</sup> In this study, p53/JNK activation and MDM2 inhibition (Figure 3) were observed in irradiated parotid gland tissues, and this may be correlated with radiation-induced ROS production. The activation of p53/JNK activation can further activate and impair proapoptotic and antiapoptotic signal transduction, respectively. A significant downregulation of Bcl-2 expression and a significant upregulation of Bax and Caspase-3 expression were observed in irradiated parotid gland tissues. On the other hand, RA significantly reversed Bax/Bcl-2 signaling and Caspase-3 expression in parotid gland tissues after IR, and these changes were correlated with the impairment of p53/JNK activation via the antioxidant effect of RA.

Fibrosis is common in advanced IR injury. Radiation-induced oxidative stress can promote the inflammatory response, which may further develop into interstitial fibrosis and increase the production of inflammatory cytokines.<sup>47</sup> Reactive oxygen species cause tissue damage and trigger several inflammatory reactions. During the inflammatory reaction process, ROS induce the production of inflammatory cytokines.<sup>48</sup> Previously, elevated levels of the pro-inflammatory factors TNF- $\alpha$ , IL-6,<sup>28</sup> and IL-2<sup>27</sup> were linked to radioactive pulmonary fibrosis and other types of pulmonary fibrosis. Recently, there has been little research on the causes of radioactivity-induced salivary gland fibrosis. In our experiment, TNF- $\alpha$ , IL-6, and IL-2 levels, like Collagen I and Collagen III levels, were significantly upregulated. On the other hand, RA significantly reversed the radiation-induced changes in TNF- $\alpha$ , IL-6, IL-2, collagen I, and collagen III expression.

All our results showed that 60 mg/kg was the minimum effective dose of RA; RA was more effective when it was administered at a dose of 60 mg/kg or 120 mg/kg than when it was administered at a dose of 30 mg/kg. A similar result was observed with a dose-effect relation curve in preliminary experiments, which showed that RA is not dose-dependent.<sup>24</sup>

This can be attributed to the fact that after RA reaches a certain dosage, the antioxidant action plateaus. In the present study, AMI had the same effects on the inhibition of oxidative stress and apoptosis but not on fibrosis. Additionally, using AMI is not convenient because of its intravenous administration and is unbearable for patients because of its side effects. Rosmarinic acid showed radioprotective effects and low toxicity when administered orally. Moreover, except for the strong acute radioprotective effect on the parotid gland after IR, RA had an obvious effect on protecting parotid gland tissues in the later stage. We speculate that RA can not only suppress apoptosis by inhibiting radiation-induced oxidative stress but also inhibit parotid gland tissue fibrosis by constraining the inflammatory response.

## Conclusions

The present study suggests that the radiation-induced enhancement of the production of ROS potentially contributes to the pathophysiology of the rat parotid glands. Rosmarinic acid treatment significantly attenuated ROS through a direct hindrance effect and the indirect activation of PGC1- $\alpha$ /NOX4 signaling. Moreover, RA reduced cell apoptosis by inhibiting p53/JNK activation and suppressed fibrosis by downregulating inflammatory factor levels in the parotid glands. Therefore, RA demonstrates superior potential for treating radiation-induced parotid gland injury.

## Authors' Note

Tingting Zhang and Chang Liu contributed equally to this work

## Declaration of Conflicting Interests

The author(s) declared no potential conflicts of interest with respect to the research, authorship, and/or publication of this article.

## Funding

The author(s) disclosed receipt of the following financial support for the research, authorship, and/or publication of this article: This work was supported by grants from the International Communication of Guangxi Medical University Graduate Education [30/02103009005X], the Basic Ability Enhancement Project of Young Teachers in Guangxi Zhuang Autonomous Region [2019KY0152], the Central Guided Local Science and Technology Development Project [GK ZY18076006], the Guangxi Key Research and Development Plan [GK AD17129013] and the Scientific Research and Technology Development Project [GKH 1599005-2-11].

## ORCID iDs

Tingting Zhang  <https://orcid.org/0000-0001-6286-999X>  
Chang Liu  <https://orcid.org/0000-0002-7047-4901>

## References

1. Rettig EM, D'Souza G. Epidemiology of head and neck cancer. *Surg Oncol Clin*. 2015;24(3):379-396.
2. Chen W, Zheng R, Baade PD, et al. Cancer statistics in China, 2015. *CA Cancer J Clin*. 2016;66(2):115-132.

3. Hakim SG, Benedek GA, Su YX, et al. Radioprotective effect of lidocaine on function and ultrastructure of salivary glands receiving fractionated radiation. *Int J Radiat Oncol Biol Phys.* 2012; 82(4):e623-e630.
4. Spratt DE, Pei X, Yamada J, Kollmeier MA, Cox B, Zelefsky MJ. Long-term survival and toxicity in patients treated with high-dose intensity modulated radiation therapy for localized prostate cancer. *Int J Radiat Oncol Biol Phys.* 2013;85(3):686-692.
5. Jellema AP, Slotman BJ, Doornaert P, Leemans CR, Langendijk JA. Impact of radiation-induced xerostomia on quality of life after primary radiotherapy among patients with head and neck cancer. *Int J Radiat Oncol Biol Phys.* 2007;69(3):751-760.
6. Hawkins PG, Lee JY, Mao Y, et al. Sparing all salivary glands with IMRT for head and neck cancer: longitudinal study of patient-reported xerostomia and head-and-neck quality of life. *Radiotherap Oncol.* 2018;126(1):68-74.
7. Chowdhury SR, Sengupta S, Biswas S, et al. Bacterial fucose-rich polysaccharide stabilizes MAPK-mediated Nrf2/Keap1 signaling by directly scavenging reactive oxygen species during hydrogen peroxide-induced apoptosis of human lung fibroblast cells. *PLoS One.* 2014;9(11):e113663.
8. Kang KA, Lee HC, Lee JJ, et al. Effects of combined radiofrequency radiation exposure on levels of reactive oxygen species in neuronal cells. *J Radiat Res.* 2013;55(2):265-276.
9. Oparka M, Walczak J, Malinska D, et al. Quantifying ROS levels using CM-H2DCFDA and HyPer. *Methods.* 2016;109:3-11.
10. Giorgio M, Trinei M, Migliaccio E, Pelicci PG. Hydrogen peroxide: a metabolic by-product or a common mediator of ageing signals? *Nat Rev Mole Cell Biol.* 2007;8(9):722.
11. Fujisawa T, Takeda K, Ichijo H. ASK family proteins in stress response and disease. *Mole Biotechnol.* 2007;37(1):13-18.
12. Tateishi Y, Sasabe E, Ueta E, Yamamoto T. Ionizing irradiation induces apoptotic damage of salivary gland acinar cells via NADPH oxidase 1-dependent superoxide generation. *Biochem Biophys Res Commun.* 2008;366(2):301-307.
13. Sarhaddi D, Tchanque-Fossuo CN, Poushanchi B, et al. Amifostine protects vascularity and improves unions in a model of irradiated mandibular fracture healing. *Plastic Reconstruct Surg.* 2013;132(6):1542-1549.
14. Hosseinimehr SJ. Trends in the development of radioprotective agents. *Drug Discov Today.* 2007;12(19-20):794-805.
15. Shanmugam PST, Nair RP, De Benedetti A, Caldito G, Abreo F, Sunavala-Dossabhoy G. Toslled kinase activator, gallic acid, promotes homologous recombinational repair and suppresses radiation cytotoxicity in salivary gland cells. *Free Rad Biol Med.* 2016; 93:217-226.
16. Akyuz M, Taysi S, Baysal E, et al. Radioprotective effect of thymoquinone on salivary gland of rats exposed to total cranial irradiation. *Head Neck.* 2017;39(10):2027-2035.
17. Makino T, Ono T, Muso E, Honda G. Inhibitory effect of *Perilla frutescens* and its phenolic constituents on cultured murine mesangial cell proliferation. *Planta Med.* 1998;64(06):541-545.
18. Jiang K, Ma X, Guo S, et al. Anti-inflammatory effects of rosmarinic acid in lipopolysaccharide-induced mastitis in mice. *Inflammation.* 2018;41(2):437-448.
19. Sotnikova R, Okruhlicova L, Vlkovicova J, et al. Rosmarinic acid administration attenuates diabetes-induced vascular dysfunction of the rat aorta. *J Pharm Pharmacol.* 2013;65(5):713-723.
20. González-Vallinas M, Reglero G, Ramírez de Molina A. Rosemary (*Rosmarinus officinalis* L.) extract as a potential complementary agent in anticancer therapy. *Nut Can.* 2015;67(8):1223-1231.
21. Lee HJ, Cho HS, Park E, et al. Rosmarinic acid protects human dopaminergic neuronal cells against hydrogen peroxide-induced apoptosis. *Toxicology.* 2008;250(2-3):109-115.
22. Wang H, Provan GJ, Helliwell K. Determination of rosmarinic acid and caffeic acid in aromatic herbs by HPLC. *Food Chem.* 2004;87(2):307-311.
23. Tavafi M. Diabetic nephropathy and antioxidants. *J Nephropathol.* 2013;2(1):20.
24. Xu W, Yang F, Zhang Y, Shen X. Protective effects of rosmarinic acid against radiation-induced damage to the hematopoietic system in mice. *J Radiat Res.* 2016;57(4):356-362.
25. Konings AW, Faber H, Vissink A, Coppes RP. Radioprotective effect of amifostine on parotid gland functioning is region dependent. *Int J Radiat Oncol Biol Phys.* 2005;63(5):1584-1591.
26. Bhattarai K, Lee HY, Kim SH, Kim HR, Chae HJ. Ixeris dentata extract increases salivary secretion through the regulation of endoplasmic reticulum stress in a diabetes-induced xerostomia rat model. *Int J Mole Sci.* 2018;19(4):1059.
27. Szema AM, Reeder RJ, Harrington AD, et al. Iraq dust is respirable, sharp, metal-laden, and induces lung inflammation with fibrosis in mice via IL-2 upregulation and depletion of regulatory T cells. *J Occup Environ Med.* 2014;56(3):243.
28. Tokat AO, Akbulut A, Billur D, et al. Montelukast attenuates radioactive I131-induced pulmonary damage on rats. *Int J Radiat Biol.* 2018;94(6):542-550.
29. Murdoch-Kinch CA, Kim HM, Vineberg KA, Ship JA, Eisbruch A. Dose-effect relationships for the submandibular salivary glands and implications for their sparing by intensity modulated radiotherapy. *Int J Radiat Oncol Biol Phys.* 2008;72(2):373-382.
30. Grundmann O, Mitchell G, Limesand K. Sensitivity of salivary glands to radiation: from animal models to therapies. *J Dent Res.* 2009;88(10):894-903.
31. Wang Y, Yang J, Yi J. Redox sensing by proteins: oxidative modifications on cysteines and the consequent events. *Antioxid Redox Signal.* 2012;16(7):649-657.
32. Kim JM, Kim JW, Choi ME, Kim SK, Kim YM, Choi JS. Protective effects of curcumin on radioiodine-induced salivary gland dysfunction in mice. *J Tissue Eng Regen Med.* 2019;13(4): 674-681.
33. Revoltella S, Baraldo G, Waltenberger B, et al. Identification of the NADPH Oxidase 4 inhibiting principle of *lycopodium europaeum*. *Molecules.* 2018;23(3):653.
34. Bonda TA, Szynaka B, Sokołowska M, et al. Interleukin 6 modulates PPAR $\alpha$  and PGC-1 $\alpha$  and is involved in high-fat diet induced cardiac lipotoxicity in mouse. *Int J Cardiol.* 2016;219:1-8.
35. Ji LL, Yeo D. Mitochondrial dysregulation and muscle disuse atrophy. *F1000Res.* 2019;8.
36. Choi YK, Kim JH, Lee DK, et al. Carbon monoxide potentiation of L-type Ca<sup>2+</sup> channel activity increases HIF-1 $\alpha$ -independent

- VEGF expression via an AMPK $\alpha$ /SIRT1-mediated PGC-1 $\alpha$ /ERR $\alpha$  axis. *Antioxid Redox Signal*. 2017;27(1):21-36.
37. Ozer M, Bilgic S, Armagan I, Savran M. Thymoquinone protection from amikacin induced renal injury in rats. *Biotech Histochemi*. 2019:1-8.
38. Bhattacharjee N, Dua TK, Khanra R, et al. Protocatechuic acid, a phenolic from *Sansevieria roxburghiana* leaves, suppresses diabetic cardiomyopathy via stimulating glucose metabolism, ameliorating oxidative stress, and inhibiting inflammation. *Front Pharm*. 2017;8:251.
39. Dhupal M, Oh JM, Tripathy DR, Kim SK, Koh SB, Park KS. Immunotoxicity of titanium dioxide nanoparticles via simultaneous induction of apoptosis and multiple toll-like receptors signaling through ROS-dependent SAPK/JNK and p38 MAPK activation. *Int J Nano Med*. 2018;13:6735.
40. Zheng T, Wang J, Zhao Y, et al. Spliced MDM2 isoforms promote mutant p53 accumulation and gain-of-function in tumorigenesis. *Nat Comm*. 2013;4:2996.
41. Zhao Y, Yu H, Hu W. The regulation of MDM2 oncogene and its impact on human cancers. *Acta Biochim Biophys Sin*. 2014;46(3):180-189.
42. Kim JY, Yu S-J, Oh HJ, Lee JY, Kim Y, Sohn J. Panaxydol induces apoptosis through an increased intracellular calcium level, activation of JNK and p38 MAPK and NADPH oxidase-dependent generation of reactive oxygen species. *Apoptosis*. 2011;16(4):347-358.
43. Sun P, Gu L, Luo J, Qin Y, Sun L, Jiang S. ROS-mediated JNK pathway critically contributes to PFOS-triggered apoptosis in SH-SY5Y cells. *Neurotoxicol Teratol*. 2019;75:106821.
44. Wang Y, Xu X, Wu X, Chen W, Huang F, Gui X. Dihydroartemisinin treatment of multiple myeloma cells causes activation of c-Jun leading to cell apoptosis. *Oncol Lett*. 2018;15(2):2562-2566.
45. Soni KK, Shin YS, Choi BR, et al. Protective effect of DA-9401 in finasteride-induced apoptosis in rat testis: inositol requiring kinase 1 and c-Jun N-terminal kinase pathway. *Drug Des Devel Ther*. 2017;11:2969.
46. Wang RS, Zhang TT, Xu ZH, et al. Injury in minipig parotid glands following fractionated exposure to 30 Gy of ionizing radiation. *Otolaryngol Head Neck Surg*. 2014;151(1):100-106.
47. Yu W, Fu J, Liu Y, Wu Y, Jiang D. Osteogenic protein-1 inhibits nucleus pulposus cell apoptosis through regulating the NF- $\kappa$ B/ROS pathway in an inflammation environment. *Biosci Rep*. 2018;38(6):BSR20181530.
48. Cheng X, Yao H, Xiang Y, et al. Effect of Angelica polysaccharide on brain senescence of Nestin-GFP mice induced by D-galactose. *Neurochem Int*. 2019;122:149-156.